MAP4K heterodimerization domains determine subcellular localisation and activity in Arabidopsis

Lixia Pan[1,2], Cassio Flavio Fonseca de Lima[1,2], Lam Dai Vu[1,2,3,4,#], Brigitte van de Cotte[1,2], Nancy De Winne[1,2], Kris Gevaert[3,4], Geert De Jaeger[1,2], Ive De Smet[1,2,*]

[1]Department of Plant Biotechnology and Bioinformatics, Ghent University, B-9052 Ghent, Belgium

[2]VIB Center for Plant Systems Biology, B-9052 Ghent, Belgium

[3]VIB-UGent Center for Medical Biotechnology, VIB, B-9000 Ghent, Belgium

[4]Department of Biomolecular Medicine, Ghent University, B-9000 Ghent, Belgium

[#]Present address: Cryptobiotix, B-9052 Ghent, Belgium

[*]Correspondence: ive.desmet@psb.vib-ugent.be

ABSTRACT

Signal transduction relies for a large part on the activity of kinases and phosphatases that control protein phosphorylation. However, we still know very little about phosphorylation-mediated signalling networks. Plant MITOGEN-ACTIVATED PROTEIN KINASE KINASE KINASE KINASEs (MAP4Ks) have recently gained more attention, given their role in a wide range of processes, including developmental processes and stress signalling. We analysed *MAP4K* expression patterns and mapped protein-MAP4K interactions in plants, revealing extensive co-expression and heterodimerization. This heterodimerization is regulated by the C-terminal, intrinsically disordered half of the MAP4K, and specifically by the coiled coil motif. The ability to heterodimerize is required for proper activity and localisation of the MAP4Ks. Taken together, our results provide novel MAP4K-interacting proteins and emphasize the functional importance for MAP4K heterodimerization. Furthermore, we identified MAP4K4/ TARGET OF TEMPERATURE3 (TOT3) and MAP4K5/ TOT3-INTERACTING PROTEIN 5 (TOI5) as novel key regulators of the cell division to elongation transition in the primary root tip.

INTRODUCTION

Dynamic and reversible phosphorylation-mediated signalling requires kinases and phosphatases. The evolutionarily conserved MITOGEN-ACTIVATED PROTEIN KINASEs (MAPK) cascades play pivotal roles in transducing extracellular stimuli into intracellular responses and typically involve three key modules (MAP3K, MAP2K and MAPK) (Zhang and Zhang, 2022). However, MAP4Ks have been positioned upstream of these classical MAP3K – MAP2K – MAPK cascades (Dan et al., 2001; Chuang et al., 2016). In the yeast *Saccharomyces cerevisiae*, the kinase Sterile 20 protein (Ste20p) was first identified as a putative regulator of a MAP kinase cascade in the mating pathway (Leberer et al., 1992). The phosphorylation of MAP3K Ste11 by Ste20p indicates that Ste20p acts as a MAP4K (Drogen et al., 2000). Based on the phylogenetic analysis of conserved domain and structure, the Ste20 family could be further divided into two subfamilies in mammals, *Drosophila*, *Caenorhabditis elegans* and other organisms: p21-activated kinase (PAK) and germinal centre kinase (GCK) subfamilies (Dan et al., 2001). The structure of the kinase domain is conserved among PAKs and GCKs, and the kinase domain contains a MAP4K signature sequence, namely GTPyWMAPEv (Dan et al., 2001). However, the location of the kinase domain is at the C-terminus in the PAKs and at the N-terminus in the GCKs (Dan et al., 2001). Seven MAP4Ks have been reported in humans, and these MAP4Ks are essential for the regulation of cell apoptosis, cell survival, cell autophagy, and cell migration (Chuang et al., 2016). Moreover, human MAP4K family members are also core components of the evolutionarily conserved Hippo signalling pathway which is important for tissue homoeostasis, and its dysregulation contributes to tumorigenesis (Meng et al., 2015).

MAP4Ks are also highly conserved in plants and in the green lineage, three major clades can be distinguished (Pan et al., 2021). In plants, the MAP4Ks have recently gained more attention, given their role in a wide range of processes, including developmental processes and

stress signalling (Pan and De Smet, 2020; Vu et al., 2021; Zhang et al., 2021b). The *Zea mays* MAIZE ATYPICAL RECEPTOR KINASE (MARK)-INTERACTING KINASE (MIK) and the *Solanum chacoense* MAP4K1 are important during embryogenesis (Pan and De Smet, 2020). BLUE LIGHT SIGNALING1 (BLUS1)/MAP4K10 is a substrate of the blue light receptor phototropins (PHOT1 and PHOT2) and regulates stomatal opening (Schnabel et al., 2018). Both SERINE/THREONINE KINASE 1 (SIK1)/MAP4K3 and TARGET OF TEMPERATURE3 (TOT3)/MAP4K4 interact with the BOTRYTIS-INDUCED KINASE 1 (BIK1) in immunity (Zhang et al., 2018; Jiang et al., 2019). SIK1/MAP4K3 is also essential for cell proliferation, expansion and root polarity (Xiong et al., 2016; Zhang et al., 2021b). TOT3/MAP4K4, TOT3-INTERACTING PROTEIN 5 (TOI5)/MAP4K5, and TOI4/MAP4K6 are involved in temperature-mediated growth (Vu et al., 2021).

While the human MAP4K interactome revealed STRN4 as a common interactor of MAP4Ks and as a key STRIPAK Complex component in Hippo pathway regulation (Seo et al., 2020), very little is known about the MAP4K protein-protein interaction network in plants. MAP4Ks display a long intrinsically disordered C-terminal half following the kinase domain (Chuang et al., 2016; Pan et al., 2021), but its role is not yet explored. Furthermore, in humans, MAP4Ks share a conserved C-terminal citron-homology domain (CNH) that is essential for protein-protein interaction, but this domain is absent in plants (Chuang et al., 2016; Pan et al., 2021). However, a conserved coiled coil motif is located at a similar position of the CNH domain in the green linage and this motif is predicted to be involved in protein localization and protein-protein interaction (Pan et al., 2021). Here, we present the interactome of a subset of plant MAP4Ks and provide experimental evidence for the role of the C-terminal half of the protein, and especially the coiled coil motif, in controlling protein-protein interactions and MAP4K subcellular localization.

RESULTS AND DISCUSSION

Arabidopsis MAP4Ks are expressed in unique and overlapping patterns

Previously, several *Arabidopsis* MAP4Ks were shown to play a role in thermomorphogenesis, stomatal opening, cell proliferation and expansion, root polarity and innate immunity (Pan and De Smet, 2020; Hosotani et al., 2021; Vu et al., 2021; Zhang et al., 2021a). However, little is known about the diverse developmental roles of MAP4Ks. In view of the increase in members throughout plant evolution of subclade III (Pan et al., 2021), which is possibly associated with several new and distinct functions for these MAP4Ks, we focused on MAP4K4 to MAP4K9 [referred to as MAP4K(4-9)] (**Fig. 1A**). To explore in which developmental processes MAP4K(4-9) could be involved, we analysed their expression patterns in a wide range of organs using *pMAP4K(4-9)::GUS* fusions. Detailed analyses of diverse plant organs revealed distinct and overlapping expression patterns in the root, shoot and flowers (**Fig. 1B-C and Fig. S1)**. Apart from *MAP4K9*, several *MAP4Ks* are co-expressed in various organs and tissues (**Fig. 1B-C**). This is in agreement with previously observed overlapping roles of, for example, TOT3/MAP4K4, TOI4/MAP4K6 and TOI5/MAP4K5 in (warm temperature-mediated) hypocotyl growth (Vu et al., 2021). Similarly, the expression patterns in the root suggest (partially) overlapping roles for TOT3 and TOI5, and for TOT3 and MAP4K8 in the primary root tip (**Fig. 1D**). Indeed, a *tot3-2 toi5-2* double mutant displayed a shorter primary root compared to the wild type control and single mutants (**Fig. 1E-F**). Primary root length is determined by cell division and elongation (Beemster and Baskin, 1998). Analysing meristem size and cell number revealed that the *tot3-2 toi5-2* double mutant has a significantly shorter primary root meristem with fewer cells, compared to the wild type control (**Fig. 1G-I**). The partially overlapping *TOT3* and *TOI5* expression pattern in the primary root tip and the *tot3-2*

toi5-2 phenotype support that TOT3 and TOI5 are key regulators of the cell division to elongation transition.

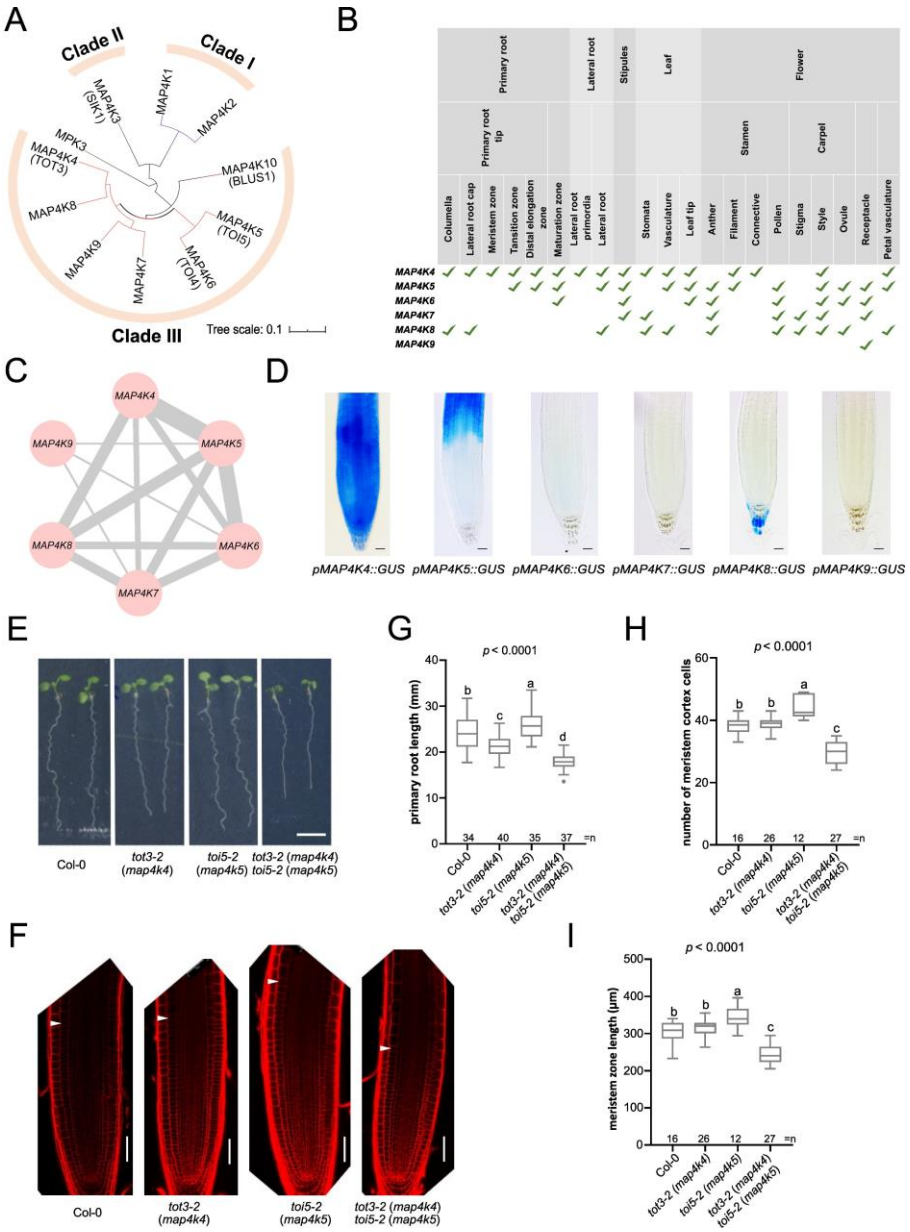

Figure 1. Expression patterns of *MAP4Ks* underpinning their function. **(A)** Cladogram of MAP4K family in *Arabidopsis*. MPK3 was used as an outgroup. Other protein names are mentioned between parentheses. **(B)** Summary of expression patterns of *MAP4K(4-9)*. See Figure S1 for representative images. **(C)** *MAP4K* co-expression network. The thickness of edges reflects the number of co-expressed organs or tissues**.** (**D**) Expression pattern of *MAP4K(4-9)* in the primary root tip. Scale bars, 20 µm. **(E-I)** MAP4K4 and MAP4K5 are key regulators of the cell division to elongation transitions. For *map4k4* and *map5k5* mutant phenotyping, *tot3-2* and *toi5-2* were used, respectively. Phenotypic assay of 5 days after germination Col-0, *tot3-2 (map4k4)*, *toi5-2* (*map4k5)* and *tot3-2 toi5-2* (*map4k4 map4k5)* seedlings grew under long day conditions at 21 °C. (**E-F**) Representative images of the primary root (E) and confocal microscopy images of primary root meristem zone (F). Scale bars, 10 mm (E) and 50 µm (F). **(G-I)** Quantification for primary root length (G), the number of cortex cells in the meristem (H) and meristem zone length (I). Box plots show a median with Tukey-based whiskers and outliers. The number of individually measured seedlings (n) is indicated above the X-axis. Letters indicate significant differences based on one-way ANOVA and Tukey's test ($p < 0.01$). The *p*-value for the genotypes is shown at the top.

Arabidopsis MAP4K interactome identifies distinct and common MAP4K-interacting proteins

To pinpoint if and how MAP4K(4-9) indeed control distinct and overlapping processes, we focused on their interacting proteins. To obtain a comprehensive understanding of the MAP4K(4-9) protein-protein interaction network, we established *Arabidopsis* cells stably expressing each MAP4K family member fused to an NGSrhino or CGSrhino tag. These *MAP4K*-expressing cells were then subjected to affinity purification coupled with mass spectrometry (AP-MS), to identify the associated proteins within each isolated protein complex. A complete list of the peptides and proteins identified in this study can be found in **Table S1**. To refine the MAP4K AP-MS data, we focused on high confidence interacting proteins (see Methods). The combined AP network embeds 179 interactions among 102 proteins, and revealed distinct and common interactors (41.3% of the interactions is shared between at least 2 MAP4Ks) (**Fig. 2A and Table S2**). Because the stable cells collected for the AP-MS analysis were grown under normal culture conditions, the identified high confidence MAP4K-interacting proteins for each MAP4K(4-9) Clade III member could be considered as the basal-state interactome of the Arabidopsis MAP4K kinase family. Gene Ontology (GO) and (predicted) localisation analyses of the high confidence MAP4K-interacting proteins suggested that they were widely distributed in the cells with different sub-cellular localization (**Fig. 2B**) and were involved in diverse molecular functions and biological processes (**Figure 2C**). The interactome revealed distinct MAP4K(4-9)-interacting proteins, but also – in line with the co-expression analysis (**Fig. 1B**) – several MAP4K(4-9)-interacting proteins that are shared between two or more MAP4Ks (**Fig. 2A**). Surprisingly, while we only detected limited overlap in the expression pattern of *MAP4K9* and *MAP4K(4-8)*, the interactome revealed a high co-

interaction between proteins interacting with MAP4K9 and MAP4K(4-8).

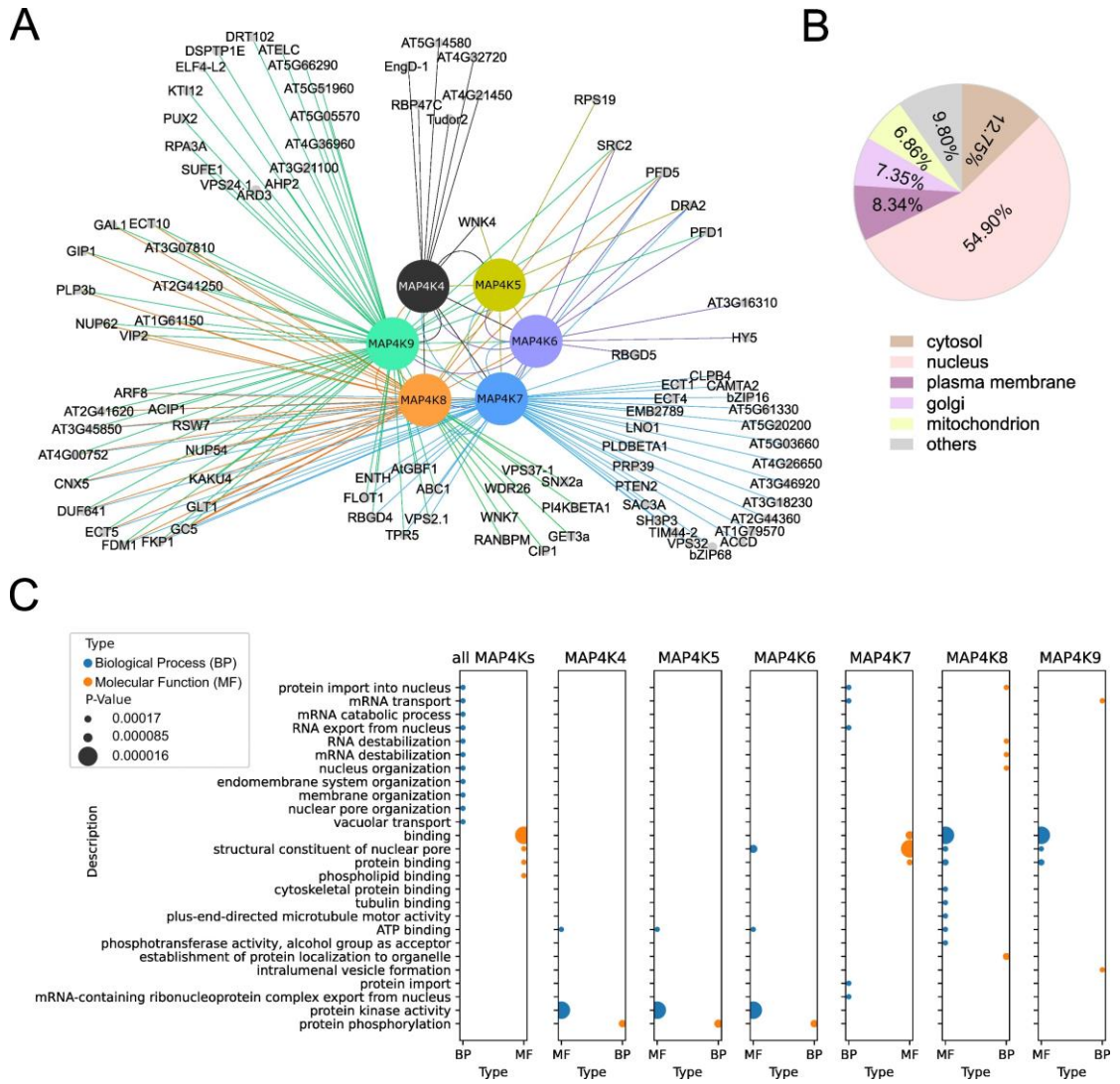

Figure 2. Affinity Purification and Mass Spectrometry (AP-MS) analysis for MAP4K protein interaction network. (A) Visualization of the MAP4Ks interactome derived from AP-MS data. **(B)** Cellular localization of MAP4K interactors based on Arabidopsis protein subcellular location data from SUBA5. **(C)** GO enrichment of MAP4K interactors in biological process and molecular function.

Arabidopsis MAP4Ks form hetero-dimers

Intriguingly, the MAP4K(4-9) basal-state interactome revealed – in line with previous research in non-plant organisms (Glantschnig et al., 2002; Jin et al., 2012; Zhou et al., 2018) – frequent hetero-dimer formation among the MAP4K family members (**Fig. 3A**). Co-immunoprecipitation (co-IP) experiments (**Fig. S2A**), yeast two-hybrid experiments (Y2H) (**Fig. S2B**) and bimolecular fluorescence complementation (BiFC) assays (**Fig. S2C**) independently confirmed interactions between several of the MAP4Ks (**Fig. 3A**). Based on

MAP4K(4-9) interactions, expression patterns and functional redundancies (Vu et al., 2021) (**Fig. 1**), it appears as if particular heterodimer combinations (or potentially higher order complexes) are associated with specific processes.

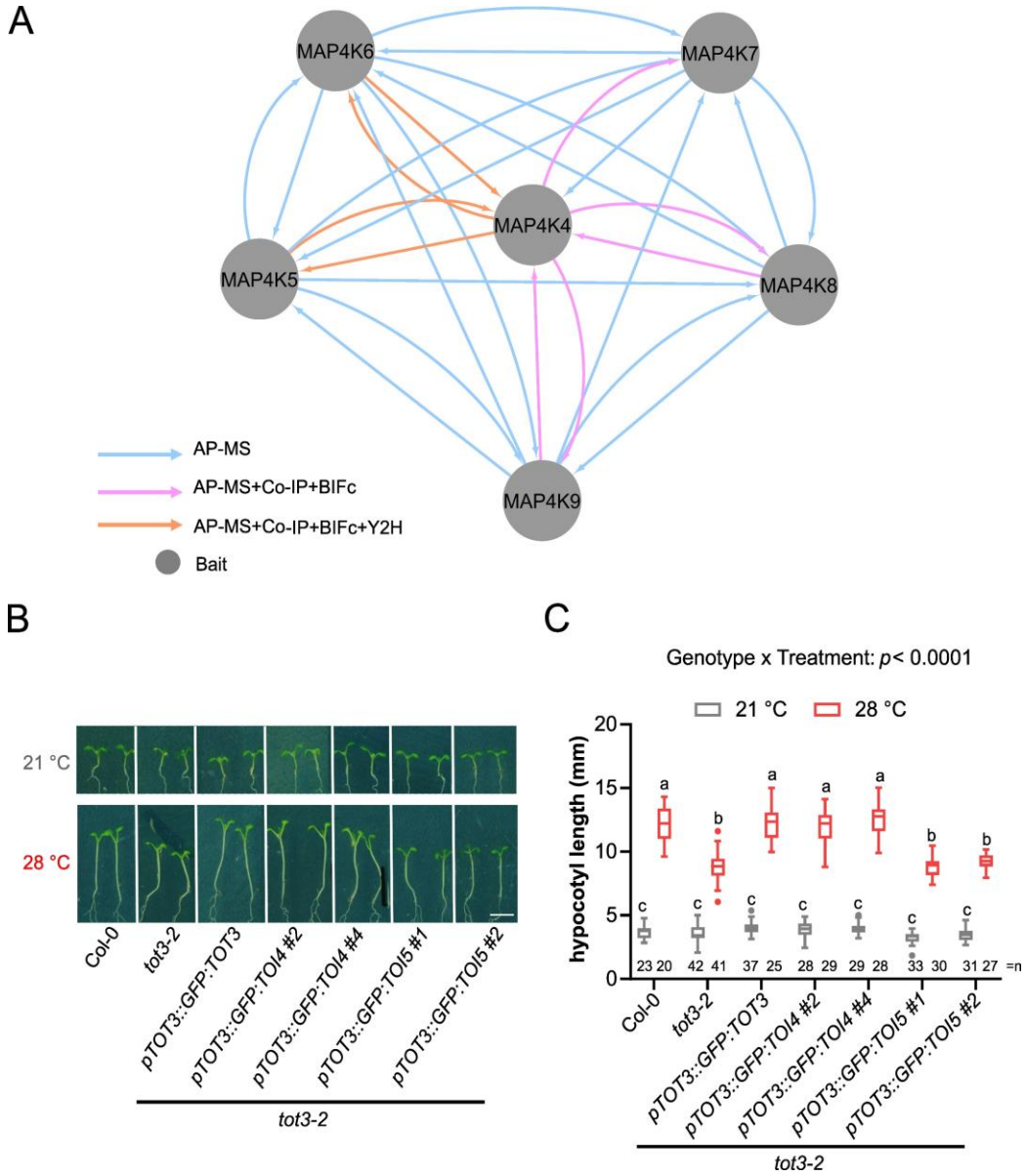

Figure 3. Arabidopsis MAP4Ks form hetero-dimers. (A) MAP4K(4-9) hetero-dimer interactions. Integrated node and edge attributes are shown next to the network. **(B-C)** Hypocotyl length for indicated lines at 21 and 28 °C in short-day conditions. Representative pictures (B) and hypocotyl length quantification (C). Scale bar, 5 mm. Box plots show median with Tukey-based whiskers and outliers. The number of individually measured seedlings (n) is indicated above the X-axis. Letters indicate significant differences based on two-way ANOVA and Tukey's test ($p < 0.01$) (C). *p*-value shown at the top.

Arabidopsis TOT3 and TOI4 are functionally interchangeable in thermomorphogenesis

Using TOT3, TOI4 and TOI5 as representative heterodimerizing MAP4Ks, we explored to what extent these MAP4Ks are interchangeable. Previously, we showed that *tot3-2* displayed a significantly shorter hypocotyl at 28 °C when compared to Col-0 (Vu et al., 2021). By expressing *TOI5* or *TOI4* under the *TOT3* promoter, we assessed the ability of TOI5 or TOI4 to rescue the *tot3-2* hypocotyl phenotype at 28 °C (**Fig. S3**). A *pTOT3::GFP:TOT3* construct complemented the *tot3-2* hypocotyl phenotype at 28 °C (**Fig. 3B-C**) (Vu et al., 2021). Similarly, a *pTOT3::GFP:TOI4* construct is able to rescue the *tot3-2* hypocotyl phenotype at 28 °C (**Fig. 3B-C**). However, the *pTOT3::GFP:TOI5* construct did not rescue the *tot3-2* hypocotyl phenotype at 28 °C (**Fig. 3B-C**). This suggested that some MAP4Ks are interchangeable, at least in the context of warm temperature-mediated hypocotyl growth, but that TOI5 requires a functional TOT3 for its activity.

C-terminal half of Arabidopsis TOT3 is required for interaction and localization

The C-terminal half from the end of the kinase domain to utmost C-terminal amino acid of MAP4Ks is largely intrinsically disordered (Pan et al., 2021). Since intrinsically disordered regions are involved in protein-protein interactions and protein localization (Lee et al., 2017; Cornish et al., 2020; Trivedi and Nagarajaram, 2022; Kibar and Vingron, 2023), we explored to what extent the MAP4K C-terminal half is necessary for hetero-dimerization and localization. For this, we again used TOT3 – TOI5 as a representative pair. Using a Y2H assay and co-IP, we first showed that removing the C-terminal half abolishes the interaction between $TOT3^{1-296}$ and TOI5 (**Fig. 4A-C**). In addition, the TOT3 protein lacking the C-terminal half also displayed a different localization, namely $GFP:TOT3^{1-305}$ accumulated more in the nucleus (**Fig. 4D**). While a *pTOT3::GFP:TOT3* construct complemented the *tot3-2* hypocotyl phenotype at 28 °C (Vu et al., 2021), a TOT3 protein variant that lacked the C-terminal half

(3×HA:TOT3$^{1–308}$) could not rescue the *tot3-2* short hypocotyl phenotype at 28 °C (**Fig. 4E-F and Fig. S3**). Previously, we identified a conserved C-terminal coiled-coil motif (TOT3$^{623-672}$) in these MAP4Ks (**Fig. 4A**) (Pan et al., 2021), which could be involved in protein-protein interactions and protein localization (Mier et al., 2017; Georgoulia and Bjelic, 2021). Here, we explored to what extent the TOT3 C-terminal coiled-coil motif is indeed necessary for TOT3 hetero-dimerization and localization. Using a Y2H assay and co-IP, we first showed that removing the coiled-coil motif abolishes the interaction between TOT3$^{1-610}$ and TOI5 (**Fig. 4B-C**). In addition, the TOT3 protein lacking the C-terminal coiled-coil motif displayed a different localization, namely GFP:TOT3$^{1-610}$ accumulated more in the nucleus (**Fig. 4D**). Furthermore, a TOT3 protein variant that lacked the C-terminal coiled-coil motif (GFP:TOT3$^{1–610}$) could not rescue the *tot3-2* short hypocotyl phenotype at 28 °C (**Fig. 4E-F and Fig. S3**). In conclusion, the C-terminal half and the C-terminal coiled-coil motif are important for TOT3 function, specifically protein-protein interactions and localization.

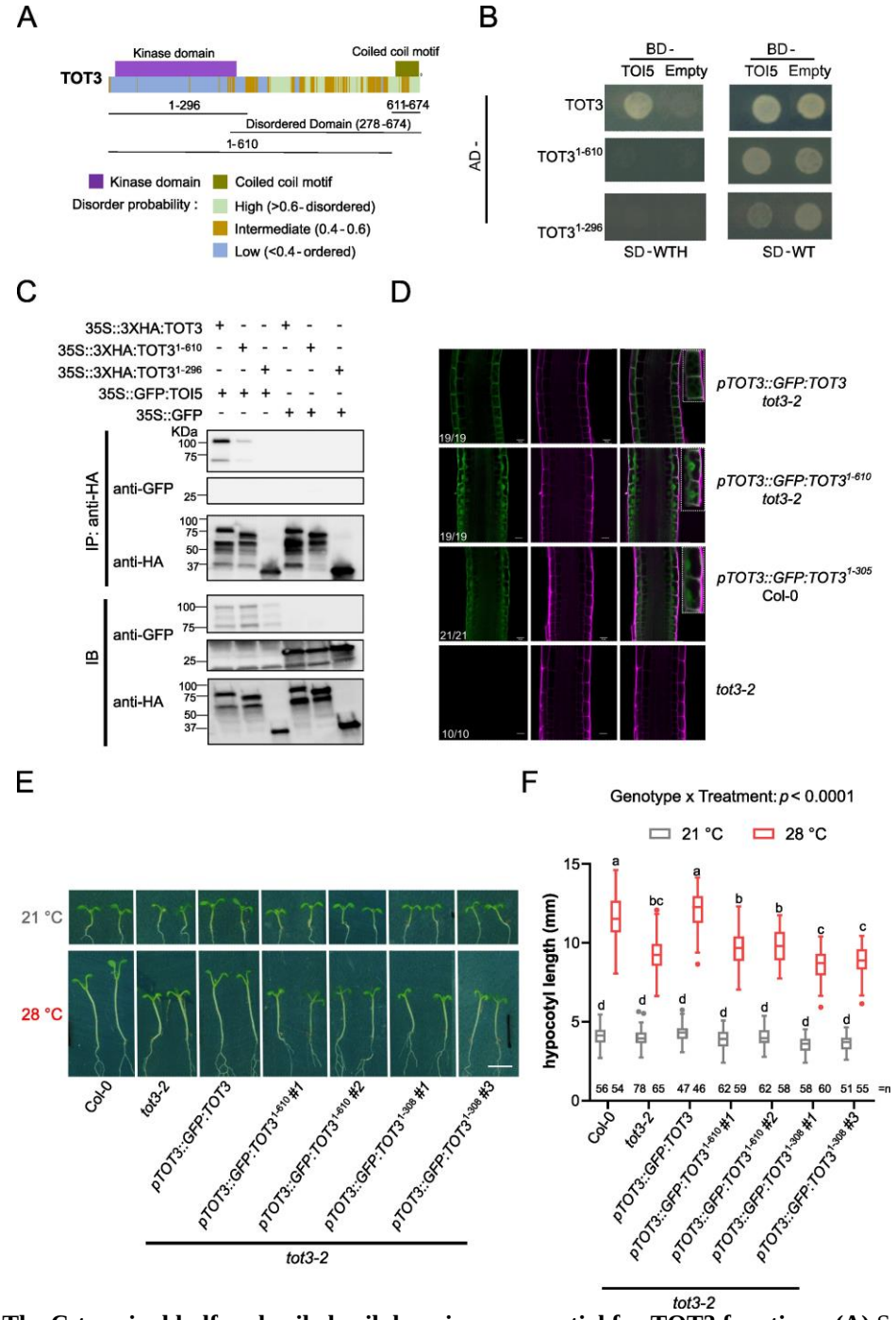

Figure 4. The C-terminal half and coiled coil domain are essential for TOT3 functions. (A) Schematic of TOT3 protein domains and motifs. **(B)** Yeast two-hybrid between TOT3 lacking the C-terminus (1-296) or the coiled coil motif (1-610) and TOI5. BD, BINDING DOMAIN; AD, ACTIVATION DOMAIN; -WT, without Leu and Trp; -WTH, without Leu, Trp and His. **(C)** Co-immunoprecipitation (co-IP) between TOT3 lacking the C-terminus (1-296) or the coiled coil motif (1-610) and TOI5. **(D)** Localization of TOT3 and TOT3 lacking the C-terminus (1-296) or the coiled coil motif (1-610) fused to GFP in the primary root meristem and transition zone. Inset shows TOT3 localisation in two cells. The numbers indicate the number of seedlings corresponding to the representative localization out of total number of seedlings analysed. Scale bar, 20 µm. Green, GFP; Magenta, propidium iodide. **(E-F)** Representative pictures (E) and hypocotyl length quantification for truncated TOT3 constructs in *tot3-2* at 21 and 28 °C in short-day conditions (F). Scale bar, 5 mm. Box plots show median with Tukey-based whiskers and outliers. The number of individually measured seedlings (n) is indicated above the X-axis. Letters indicate significant differences based on two-way ANOVA and Tukey's test ($p < 0.01$) (F). *p*-value shown at the top.

CONCLUSION

Previously, we identified the membrane-associated protein kinase MAP4K4/TOT3 as a new key player in plant responses to warm temperature (Vu et al., 2021). We showed that MAP4K4/TOT3 interacts with related MAP4Ks (MAP4K6/TOI4 and MAP4K5/TOI5) and that these related kinases also play a role in thermomorphogenesis (Vu et al., 2021). In this study, we provide valuable insight into the functional roles and interactions of MAP4K proteins within the context of plant cell biology and thermomorphogenesis. One notable aspect is the identification of distinct and overlapping gene expression patterns of *MAP4Ks* in different organs, tissues and cells. This implies that these MAP4K proteins, likely as heterodimers, may be involved in multiple biological processes. For instance, we demonstrated that MAP4K4/TOT3 and MAP4K6/TOI4 are exchangeable in thermomorphogenesis. Since MAP4K4/TOT3, for example, also regulates plant innate immunity (Jiang et al., 2019), it will be intriguing to explore of similar heterodimers also function in that process. The expression of both *MAP4K7* and *MAP7K8* in stomata and pollen raises intriguing questions about their potential contributions to stomata development and fertilization. Here, we also pinpointed a role for the MAP4K4/TOT3 – MAP4K5/TOI5 pair in primary root growth. Several hormone and nutrient signalling pathways play a key role in the cell division to elongation transition in the primary root (Zluhan-Martínez et al., 2021; Jia et al., 2022), and it remains to be analysed if and how TOT3 interacts with these pathways. We previously showed that TOT3 impinges on brassinosteroid-mediated hypocotyl growth control under warm temperature (Vu et al., 2021), and possibly TOT3 has a similar role in the primary root. In addition, the MAP4Ks protein-protein interaction landscape identified approximately 100 MAP4K interactors, which further supports their involvement in a wide range of cellular events. This opens up new avenues for investigating the diverse roles of MAP4Ks in various signalling pathways, including plant innate immunity and root architecture.

The role of the intrinsically disordered C-terminal half and of the coiled coil domain in Arabidopsis MAP4K heterodimer formation and localisation, can also provide valuable insight on these cellular processes in other organisms. Indeed, the coiled coil domain of MAP4K4/TOT3 is vital for TOT3 interactions with other MAP4Ks to control thermomorphogenesis. It is, however, still an open question how the MAP4K coiled coil domain impacts the larger MAP4K interactome. Our phosphoproteome data on MAP4K4/TOT3 indicated that this intrinsically disordered C-terminal half is also subjected to intense phosphorylation impacting the activity of the protein (Xu et al., 2023; Willems et al., 2019; Vu et al., 2021) (**Fig. S4**). How phosphorylation impacts MAP4K heterodimer formation and localisation will be an area of future study.

Taken together, this study advances our understanding of MAP4K proteins and their roles in various biological processes and underscores the importance of exploring the interactions and functions of these proteins in different cellular contexts.

MATERIALS AND METHODS

Plant materials and growth conditions

All Arabidopsis plants used in this study were in the Col-0 reference accession genetic background and referred to as wild-type. The following Arabidopsis mutants were used in this study: *tot3-2, toi5-2* and double mutant *tot3-2 toi5-2* (Vu et al., 2021). Seeds were surface-sterilized by 70% ethanol, plated on half strength Murashige and Skoog (MS) medium with 1% agar (per litre: 2.15 g of MS salts, 0.1 g of myo-inositol, 0.5 g of MES, 10 g of sucrose and 8 g of plant tissue culture agar; pH 5.7). Seeds were stratified at 4 °C for 2 days in the dark and then moved to 21°C under continuous light for germination for 48 h. For GUS staining of young seedlings and western blot, seedlings grew in the continues light growth chamber at 21 °C for 5 days after germination. For GUS staining of flowers, seedlings grew on half strength

Murashige and Skoog (MS) medium for two weeks, and were then transferred to soil for another 4 weeks. For primary root phenotyping, germinated seedlings grown under long day conditions (16 h day / 8 h night) at 21 °C for 5 days. For hypocotyl phenotyping, germinated seedlings were grown under short day conditions (8 h day / 16 h night) at 21 °C or at 28 °C for 7 days. Images were taken with a Canon scanner and measurements performed using Fiji ImageJ (https://imagej.net/Fiji).

Generation of constructs and transgenic lines

PCR was performed using iProof™ High-Fidelity DNA Polymerase or Q5® High-Fidelity polymerase according to the instruments with primers pairs (**Table S**3). The CDSs of *MAP4K7* (1785 basepairs), *MAP4K8* (4721 basepairs) and *MAP4K9* (2878 basepairs) were synthesized (Twist Bioscience, USA). GoldenGate system (Lampropoulos et al., 2013) and Gateway cloning system (Hartley, 2000; Karimi et al., 2007) were used to generated the constructs in this study (**Table S**4). Plant constructs were transformed into *Agrobacterium tumefaciens* C58C1 using the freeze-thaw method (Weigel and Glazebrook, 2006). Plant transformation was performed using the floral dip method (Clough and Bent, 1998).

Phylogenetic tree of Arabidopsis MAP4Ks

MITOGEN-ACTIVATED PROTEIN KINASE 3 (MPK3) was added as an outgroup of MAP4Ks. Alignment of all Arabidopsis MAP4K and MPK3 protein sequences was performed in CLC Main Workbench 20.03 (CLC Bio-Qiagen, Aarhus, Denmark) with default setup. Subsequently, the phylogenetic tree was visualized using the Interactive Tree Of Live version 4 (iTOL) (Letunic and Bork, 2019).

Histochemical β-Glucuronidase (GUS) staining

Seedlings (7 DAG) or flowers (6 weeks old plants) were fixated in cold 90% (v/v) acetone for 1 h and then rinsed twice with NT buffer (100 mM Tris/50 mM NaCl). Then, samples were transferred to a GUS-solution (500 µL 100 mM $K_3[Fe(CN)_6]$ + 600 µL 500 µg/ml X-Gluc + 28.8 ml NT-buffer), and incubated at 37 °C in darkness until sufficiently strong staining was observed. The plants were rinsed with NT buffer to remove the staining agents and mounted on glass slides in 80% (v/v) lactic acid. Finally, pictures were taken using an Olympus BX51 microscope.

Affinity purification (AP) analysis

AP analysis for MAP4K4/TOT3 was described previously (Vu et al., 2021). For the other MAP4Ks, the Gateway system was used to recombine the *MAP4K5* CDS (2178 basepairs), *MAP4K6* CDS (2136 basepairs), *MAP4K8* genomic DNA (4721 basepairs), and *MAP4K9* genomic DNA (2878 basepairs) in to pGNGSrhino vector (Invitrogen). *MAP4K7* CDS was recombined in to both pGNGSrhino and pGCGSrhino vectors separately. The constructs were transformed into *Arabidopsis thaliana* PSB-D cells (Van Leene et al., 2015). Three GSrhino based pull downs on Arabidopsis cell suspension cultures expressing each of the GS^{rhino} tagged baits were performed as described (Van Leene et al., 2022) using 1% digitonin in extraction buffer and 0.2% digitonin in wash buffer. On-bead digested samples were analyzed on a Q Exactive (ThermoFisher Scientific) and co-purified proteins were identified with Mascot (Matrix Science) using standard procedures(Van Leene et al., 2015) . The identified protein list was filtered versus a large dataset of AP-MS experiments, similarly as described before (Van Leene et al., 2015; Van Leene et al., 2022). The baits in the large AP-MS dataset are functionally grouped into baitgroups, and baits related to the bait of interest are removed from this large dataset before comparison. For each identified protein a Normalized Spectral Abundance Factor (NSAF) is calculated. The Ln-transformed mean NSAF of all proteins identified are compared to the Ln-transformed mean NSAF of the same protein in the large

dataset by a two-tailed t-test. Proteins that comply with the following criteria are considered significantly enriched vs the large dataset and are retained in the Filtered set: i) two-peptide identifications present in at least two out of three replicates are significantly enriched with a mean NSAF ratio ≥ 10 AND a -Log_{10}(*p*-value) ≥ 10 or with a mean NSAF ratio ≥ 20 AND a -Log_{10}(*p*-value) ≥ 8, ii) one-peptide identifications present in at least three replicates, that were detected in at least one replicate with two peptides, are significantly enriched with a mean NSAF ratio ≥ 20 AND a -Log_{10}(p-value) ≥ 50.

Gene Ontology (GO) analysis

GO enrichment analyses were performed using Dicots PLAZA 5.0 workbench (Van Bel et al., 2022). All detected putative MAP4K interactors were enriched for GO categories by using the whole species as the background model. Significance settings were set at a p-value cut-off <0.05 and Bonferroni correction for multiple testing was used. Cellular localization of all interactors was determined through SUBA5 (https://suba.live/).

Tobacco infiltration

For transient co-agroinfiltration of tobacco leaves, *Agrobacteria* containing the indicated constructs and P19 were grown in 5 ml LB supplemented with appropriate antibiotics at 28 °C for 1-2 days. Then 500 µl was inoculated in 10 ml LB supplemented with 10 mM MES pH 5.6, 10 µM acetosyringone as well as the antibiotics and grown at 28 °C overnight. The pellet was spun down and resuspended with infiltration buffer (10 mM $MgCl_2$, 10 mM MES [pH 5.6], 100 µM acetosyringone) to a final OD600 of 1.0. Equal volumes of three agrobacteria with selected constructs were mixed well and the mix was infiltrated in 5-6 weeks old tobacco leaves using a syringe. The signal was checked by confocal microscopy after 72 h to make sure the protein expressed well.

Co-immunoprecipitation (co-IP)

Total proteins were extracted with buffer containing 150 mM Tris·HCl, pH 7.5, 150 mM NaCl, 10% glycerol, 100 mM EDTA, 1 mM sodium molybdate, 1 mM NaF, 10 mM DTT, 1% NP-40, 1mM PMSF and EDTA-free protease inhibitor mixture complete (Roche). The protein concentration was measured using the Qubit™ Protein Assay Kit (Qubit™ Protein Assay Kit) and an equal amount of total protein was used for immunoprecipitation. 25 µl of pre-equilibrated HA-Trap®_MA beads (Thermo Fisher) was prewashed 3 times with 700 µl wash buffer (20 mM Tris·HCl, pH 7.5, 150 mM NaCl and 0.5% NP-40). The protein homogenates were incubated with HA-Trap®_MA beads and rotated for 2 h at 4°C to maximize protein binding. Subsequently, the solution was removed, the beads were washed three times with wash buffer (20 mM Tris-HCl pH 7.5, 150 mM NaCl and 0.5% NP-40). Finally, 1x sample buffer (Bio Rad) was added to elute protein from the beads.

Western blot

Method for protein extraction described as for co-IP. Protein samples were heated at 70 °C for 10 min, then separated on 4–20% SDS-PAGE stain-free protein gel (Bio-Rad Laboratories, Inc., USA), followed by transferring onto a Trans-Blot® Turbo™ Mini PVDF Transfer Packs (Bio-Rad Laboratories, Inc., USA). For blocking and antibody dilutions, 5% milk powder in TBST solution was used. For protein detection the following antibodies were used: monoclonal anti-GFP horseradish peroxidase coupled (1:5,000; Miltenyi Biotech), anti-HA (1:5000; abcam).

Bimolecular fluorescence complementation (BiFC)

The 2 in 1 BIFC analysis were performed according to the protocol described previously (Mehlhorn et al., 2018). For this, constructs containing two gene sequences of interest were introduced into the pBiFCt-2in1-NN vector by Gateway system (**Table S4**). Constructs were transferred to *Agrobacterium tumefaciens* C58 cells for tobacco infiltration. Tobacco leaf infiltration followed the protocol described in the method of ***Tobacco infiltration*** section. After 3 days, leaf disks were collected for confocal imaging using Leica SP8 confocal microscope. Images were captured with a hybrid detector (HyD) at 488 nm laser excitation and 500 nm-540 nm long-pass emission for YFP and 561 nm laser excitation and 590–640 nm long-pass emission for RFP. Gating technology was applied for autofluorescence removal.

Yeast two-hybrid assay (Y2H)

Y2H analysis were performed using the GAL4 system. The bait protein was expressed as a fusion to the DNA binding domain (DNA-BD) which is in pGBT9 gate, while the prey protein was expressed as a fusion to the domain (AD) in pGAD424 gate. Bait and prey plasmids were co-transformed into the *Saccharomyces cerevisiae* strain PJ69-4A. The transformants were selected by their growth on synthetic dextrose (SD) minimal medium lacking tryptophan (Trp) and leucine (Leu) (SD-WT medium), which are the nutritional selection markers for pGBT9 and pGAD424, respectively. We selected three positive independent transformants grown in the SD-WT liquid medium overnight at 30 °C, and diluted the overnight culture to 1/10. The positive interaction of expressed fusion proteins was then determined by 1/10 overnight cultures' growth on SD lacking Trp, Leu and histidine (His) (SD-WTH medium) at 30 °C for at least 3 days.

Confocal microscope imaging

Seedlings were grown on continuous light at 21 °C conditions for 5 days after germination, and then stained in 10 mg L^{-1} propidium iodide for 2 min and rinsed in water for 30 s. Confocal microscopy was performed using a Leica SP8 inverted confocal microscope. GFP was excited at 488 nm and detected at 498–530 nm. Propidium iodide was excited at 561 nm and detected at 578–640 nm.

DATA AVAILABILITY

All material will be made available upon reasonable request to the corresponding author (ive.desmet@psb.vib-ugent.be).

ACKNOWLEDGEMENTS

This work was supported by the Research Foundation, Flanders (FWO.OPR.2019.0009.01). LP was supported by the China Scholarship Council for a predoctoral fellowship (201806870020) and by a UGent BOF doctoral mandate (01CD0523). LDV was supported by a UGent BOF postdoctoral mandate (01P12219).

AUTHOR CONTRIBUTIONS

Conceptualization, L.P., L.D.V. and I.D.S.; investigation, L.P. C.F.F.d.L., L.D.V., B.v.d.C., N.D.W.; writing – original draft, L.P and I.D.S.; writing – review & editing, all authors; supervision, G.D.J., K.G. and I.D.S.

DECLARATION OF INTERESTS

The authors declare no competing interests.

REFERENCES

Beemster GTS, Baskin TI (1998) Analysis of Cell Division and Elongation Underlying the Developmental Acceleration of Root Growth in Arabidopsis thaliana 1. Plant Physiol **116**: 1515–1526

Van Bel M, Silvestri F, Weitz EM, Kreft L, Botzki A, Coppens F, Vandepoele K (2022) PLAZA 5.0: extending the scope and power of comparative and functional genomics in plants. Nucleic Acids Res **50**: D1468–D1474

Chuang H-C, Wang X, Tan T-H (2016) MAP4K Family Kinases in Immunity and Inflammation. pp 277–314

Clough SJ, Bent AF (1998) Floral dip: a simplified method forAgrobacterium-mediated transformation ofArabidopsis thaliana. Plant J **16**: 735–743

Cornish J, Chamberlain SG, Owen D, Mott HR (2020) Intrinsically disordered proteins and membranes: a marriage of convenience for cell signalling? Biochem Soc Trans **48**: 2669–2689

Dan I, Watanabe NM, Kusumi A (2001) The Ste20 group kinases as regulators of MAP kinase cascades. Trends Cell Biol **11**: 220–230

Drogen F, O'Rourke SM, Stucke VM, Jaquenoud M, Neiman AM, Peter M (2000) Phosphorylation of the MEKK Ste11p by the PAK-like kinase Ste20p is required for MAP kinase signaling in vivo. Curr Biol **10**: 630–9

Georgoulia PS, Bjelic S (2021) Prediction of Protein-Protein Binding Interactions in Dimeric Coiled Coils by Information Contained in Folding Energy Landscapes. Int J Mol Sci. doi: 10.3390/ijms22031368

Glantschnig H, Rodan GA, Reszka AA (2002) Mapping of MST1 Kinase Sites of

Phosphorylation. J Biol Chem **277**: 42987–42996

Hartley JL (2000) DNA Cloning Using In Vitro Site-Specific Recombination. Genome Res **10**: 1788–1795

Hosotani S, Yamauchi S, Kobayashi H, Fuji S, Koya S, Shimazaki K-I, Takemiya A (2021) A BLUS1 kinase signal and a decrease in intercellular CO2 concentration are necessary for stomatal opening in response to blue light. Plant Cell **33**: 1813–1827

Jia Z, Giehl RFH, von Wirén N (2022) Nutrient-hormone relations: Driving root plasticity in plants. Mol Plant **15**: 86–103

Jiang Y, Han B, Zhang H, Mariappan KG, Bigeard J, Colcombet J, Hirt H (2019) MAP4K4 associates with BIK1 to regulate plant innate immunity. EMBO Rep **20**: e47965

Jin Y, Dong L, Lu Y, Wu W, Hao Q, Zhou Z, Jiang J, Zhao Y, Zhang L (2012) Dimerization and cytoplasmic localization regulate Hippo kinase signaling activity in organ size control. J Biol Chem **287**: 5784–96

Karimi M, Depicker A, Hilson P (2007) Recombinational Cloning with Plant Gateway Vectors. Plant Physiol **145**: 1144–1154

Kibar G, Vingron M (2023) Prediction of protein-protein interactions using sequences of intrinsically disordered regions. Proteins **91**: 980–990

Lampropoulos A, Sutikovic Z, Wenzl C, Maegele I, Lohmann JU, Forner J (2013) GreenGate - A Novel, Versatile, and Efficient Cloning System for Plant Transgenesis. PLoS One **8**: e83043

Leberer E, Dignard D, Harcus D, Thomas DY, Whiteway M (1992) The protein kinase homologue Ste20p is required to link the yeast pheromone response G-protein beta gamma subunits to downstream signalling components. EMBO J **11**: 4815–4824

Lee S, Devamani T, Song HD, Sandhu M, Larsen A, Sommese R, Jain A, Vaidehi N,

Sivaramakrishnan S (2017) Distinct structural mechanisms determine substrate affinity and kinase activity of protein kinase Cα. J Biol Chem **292**: 16300–16309

Van Leene J, Eeckhout D, Cannoot B, De Winne N, Persiau G, Van De Slijke E, Vercruysse L, Dedecker M, Verkest A, Vandepoele K, et al (2015) An improved toolbox to unravel the plant cellular machinery by tandem affinity purification of Arabidopsis protein complexes. Nat Protoc **10**: 169–187

Van Leene J, Eeckhout D, Gadeyne A, Matthijs C, Han C, De Winne N, Persiau G, Van De Slijke E, Persyn F, Mertens T, et al (2022) Mapping of the plant SnRK1 kinase signalling network reveals a key regulatory role for the class II T6P synthase-like proteins. Nat Plants **8**: 1245–1261

Letunic I, Bork P (2019) Interactive Tree Of Life (iTOL) v4: recent updates and new developments. Nucleic Acids Res **47**: W256–W259

Mehlhorn DG, Wallmeroth N, Berendzen KW, Grefen C (2018) 2in1 Vectors Improve In Planta BiFC and FRET Analyses. pp 139–158

Meng Z, Moroishi T, Mottier-Pavie V, Plouffe SW, Hansen CG, Hong AW, Park HW, Mo J-S, Lu W, Lu S, et al (2015) MAP4K family kinases act in parallel to MST1/2 to activate LATS1/2 in the Hippo pathway. Nat Commun **6**: 8357

Mier P, Alanis-Lobato G, Andrade-Navarro MA (2017) Protein-protein interactions can be predicted using coiled coil co-evolution patterns. J Theor Biol **412**: 198–203

Pan L, Fonseca De Lima CF, Vu LD, De Smet I (2021) A Comprehensive Phylogenetic Analysis of the MAP4K Family in the Green Lineage. Front Plant Sci. doi: 10.3389/fpls.2021.650171

Pan L, De Smet I (2020) Expanding the Mitogen-Activated Protein Kinase (MAPK) Universe: An Update on MAP4Ks. Front Plant Sci. doi: 10.3389/fpls.2020.01220

Schnabel J, Hombach P, Waksman T, Giuriani G, Petersen J, Christie JM (2018) A

chemical genetic approach to engineer phototropin kinases for substrate labeling. J Biol Chem **293**: 5613–5623

Seo G, Han H, Vargas RE, Yang B, Li X, Wang W (2020) MAP4K Interactome Reveals STRN4 as a Key STRIPAK Complex Component in Hippo Pathway Regulation. Cell Rep **32**: 107860

Trivedi R, Nagarajaram HA (2022) Intrinsically Disordered Proteins: An Overview. Int J Mol Sci. doi: 10.3390/ijms232214050

Vu LD, Xu X, Zhu T, Pan L, van Zanten M, de Jong D, Wang Y, Vanremoortele T, Locke AM, van de Cotte B, et al (2021) The membrane-localized protein kinase MAP4K4/TOT3 regulates thermomorphogenesis. Nat Commun **12**: 2842

Weigel D, Glazebrook J (2006) Transformation of Agrobacterium Using the Freeze-Thaw Method. Cold Spring Harb Protoc **2006**: pdb.prot4666

Willems P, Horne A, Van Parys T, Goormachtig S, De Smet I, Botzki A, Van Breusegem F, Gevaert K (2019) The Plant PTM Viewer, a central resource for exploring plant protein modifications. Plant J **99**: 752–762

Xu X, Praat M, Pizzio G, Jiang Z, Driever S, Wang R, van de Cotte B, Villers S, Gevaert K, Leonhardt N, et al (2023) A conserved signaling axis integrates conflicting environmental drought and heat signals to control stomatal aperture in plants. Res Sq. doi: https://doi.org/10.21203/rs.3.rs-3228667/v1

Xiong J, Cui X, Yuan X, Yu X, Sun J, Gong Q (2016) The Hippo/STE20 homolog SIK1 interacts with MOB1 to regulate cell proliferation and cell expansion in Arabidopsis. J Exp Bot **67**: 1461–75

Zhang LL, Shao YJ, Ding L, Wang MJ, Davis SJ, Liu JX (2021a) XBAT31 regulates thermoresponsive hypocotyl growth through mediating degradation of the thermosensor ELF3 in Arabidopsis. Sci Adv **7**: eabf4427

Zhang M, Chiang Y-H, Toruño TY, Lee D, Ma M, Liang X, Lal NK, Lemos M, Lu Y-J, Ma S, et al (2018) The MAP4 Kinase SIK1 Ensures Robust Extracellular ROS Burst and Antibacterial Immunity in Plants. Cell Host Microbe **24**: 379–391.e5

Zhang M, Zhang S (2022) Mitogen-activated protein kinase cascades in plant signaling. J Integr Plant Biol. doi: 10.1111/jipb.13215

Zhang P, Yu X, Bai J, Gong Q (2021b) The Arabidopsis STE20/Hippo kinase SIK1 regulates polarity independently of PIN proteins. Biochem Biophys Res Commun **549**: 21–26

Zhou Y, Hong T, Tong L, Liu W, Yang X, Luo J, Wang F, Li J, Yan L (2018) Astragalus polysaccharide combined with 10-hydroxycamptothecin inhibits metastasis in non-small cell lung carcinoma cell lines via the MAP4K3/mTOR signaling pathway. Int J Mol Med **42**: 3093–3104

Zluhan-Martínez E, López-Ruíz BA, García-Gómez ML, García-Ponce B, de la Paz Sánchez M, Álvarez-Buylla ER, Garay-Arroyo A (2021) Integrative Roles of Phytohormones on Cell Proliferation, Elongation and Differentiation in the Arabidopsis thaliana Primary Root. Front Plant Sci **12**: 659155